Journal of Earth Science, *Vol. 31*, *No. 4*, *p. 668–682*, *August 2020* *ISSN 1674-487X*
Printed in China
https://doi.org/10.1007/s12583-020-1323-9

A New Discovery of Ag-Pb-Zn Mineralization via Modern Portable Analytical Technology and Stream Sediment Data Processing Methods in Dajiacuo Area, Western Tibet (China)

Xiaojia Jiang[1], **Xin Chen**[1], **Shunbao Gao**[*2], **Youye Zheng**[1, 3], **Huan Ren**[3], **Denghui Han**[1], **Chenchen Yan**[1], **Junsheng Jiang**[4]

1. *Faculty of Earth Resources*, *China University of Geosciences*, *Wuhan* 430074, *China*
2. *Institute of Geological Survey*, *China University of Geosciences*, *Wuhan* 430074, *China*
3. *State Key Laboratory of Geological Processes and Mineral Resources*, *School of Earth Science and Resources*, *China University of Geosciences*, *Beijing* 100083, *China*
4. *Wuhan Center*, *China Geological Survey*, *Wuhan* 430205, *China*

Xiaojia Jiang: https://orcid.org/0000-0002-6949-6214; Shunbao Gao: https://orcid.org/0000-0001-5853-3692

ABSTRACT: Tibet, which is rich in mineral resources, is a treasure trove for geological explorers. However, prospecting work has been slow, especially in the western part, due to the precipitous terrain, changeable climate and low access. Hence, modern advanced field analytical technology and effective data processing methods play significant roles in rapid and efficient exploration in Tibet. In this paper, spectrum-area fractal modeling and portable X-ray fluorescence analysis (pXRFA) were used to identify and verify geochemical anomalies associated with Ag-Pb-Zn mineralization based on a stream-sediment dataset of 39 elements in the Dajiacuo-Xurucuo region of western Tibet. First, staged factor analysis (SFA) was used to obtain the Ag-Pb-Zn-Cd geochemical assemblage. Second, the first-factor pattern obtained using SFA was dissociated by a spectrum-area (S-A) fractal model and a digital elevation model (DEM)-based geochemical model (DGM) was constructed. Finally, the sections of Ag, Cd, Pb, and Zn were obtained using pXRFA. The results show that Ag-Pb-Zn-Cd enrichment zones were mostly located around the contact belt of volcanic rocks and intrusions, or along SE-NW trending faults. Considering the variable terrain and catchment basin, the extension of long axes of Ag-Pb-Zn-Cd anomalies into higher elevation areas that are favorable for Ag-Pb-Zn mineralization should be investigated. Anomaly maps created with the aid of a DGM show promising potential for mineralization in the Dajiacuo-Xurucuo region, and abundant Ag-Pb-Zn mineralization was identified with the assistance of pXRFA in the source areas for the geochemical anomalies in the Dajiacuo. We conclude that SFA and the S-A fractal model constitute a valid tool to identify or verify geochemical anomalies in areas of low-density stream-sediment sampling. The pXRFA can accurately determine the source of geochemical anomalies and improve anomaly verification efficiency.

KEY WORDS: digital elevation model, portable X-ray fluorescence analysis, spectrum-area fractal model, staged factor analysis, Tibet.

0 INTRODUCTION

The Himalayan-Tibetan orogenic belt originated from the collision of the Indian-Asian Continent in the Early Tertiary and the subsequent northward movement of the Indian Continent (Fig. 1a; Zhao et al., 2019; Xu et al., 2016; Yin and Harrison, 2000; Allégre et al.,1984; Dewey and Burke, 1973). This complex tectonic movement provides an excellent geological background for metallogenesis in Tibet (Gao et al., 2019; Long et al., 2019; Gao, 2015). However, due to the extreme high elevations 4 000 m on average), hypoxic conditions, rugged and challenging terrain, short working period (available from June to October) and variable climate (Kang et al., 2010), there are many difficulties for geological work and mineral exploration in western Tibet, such as the weak essential geological work and the apparent backward in mineral exploration (Li and Wu, 2018).

Based on the above factors, there are some unsolved problems in traditional geochemical methods. Although conventional methods play a vital role in the exploration of minerals (Xi and Li, 2012), as sampling density increases, these methods (especially stream sediment surveys) may lead to multiple samples from the same area, prolonging the prospecting time, increasing prospecting cost and reducing prospecting

*Corresponding author: gaoshunbao2002@163.com

Manuscript received February 8, 2020.
Manuscript accepted April 6, 2020.

Jiang, X. J., Chen, X., Gao, S. B., et al., 2020. A New Discovery of Ag-Pb-Zn Mineralization via Modern Portable Analytical Technology and Stream Sediment Data Processing Methods in Dajiacuo Area, Western Tibet (China). *Journal of Earth Science*, 31(4): 668–682. https://doi.org/10.1007/s12583-020-1323-9. http://en.earth-science.net

efficiency. Besides, traditional data processing methods have advantages when searching for intense, significant and complete geochemical anomalies (Wang and Chen, 2015). Nevertheless, they are limited by intricate spatial patterns and weak and small anomalies in western Tibet, which leads to an inability to quickly localize a deposit. Laboratory analysis has shown, however, that fractal/multifractal models combined with multivariate statistical analysis can play significant roles in identifying complex spatial patterns, separating anomalies and background, and reducing the working range of anomalies (Zhao et al., 2016; Zuo and Wang, 2016; Ke et al., 2015; He et al., 2013; Cheng, 2012), but they don't improve prospecting efficiency because sample data can not be obtained from the field in real-time (Lemière, 2018).

In recent research, portable X-ray fluorescence analysis (pXRFA) has become a pivotal technique for field or mobile geochemical analysis (Lemière, 2018). However, this technique can only detect elements (e.g., Ag, As, Cu, Cd, Pb, Sb, Zn, etc.) in the periodic table, effectively (Druzbicka and Craw, 2013; Kovács et al., 2006). However, this technology provides near real-time decision support for field decisions (such as exploration and mining), which is a cost-effective alternative to traditional laboratory analysis, and effectively deals with severe and remote field conditions (Lemière, 2018; Newlander et al., 2015).

In this study, we identified potential geochemical anomalies and verified potential ore related to Ag-Pb-Zn mineralization in the Dajiacuo-Xurucuo area using staged factor analysis (SFA), a digital elevation model (DEM), a spectrum-area fractal model (S-A) and portable X-ray fluorescence analysis (pXRFA). We detailed the process of using modern portable

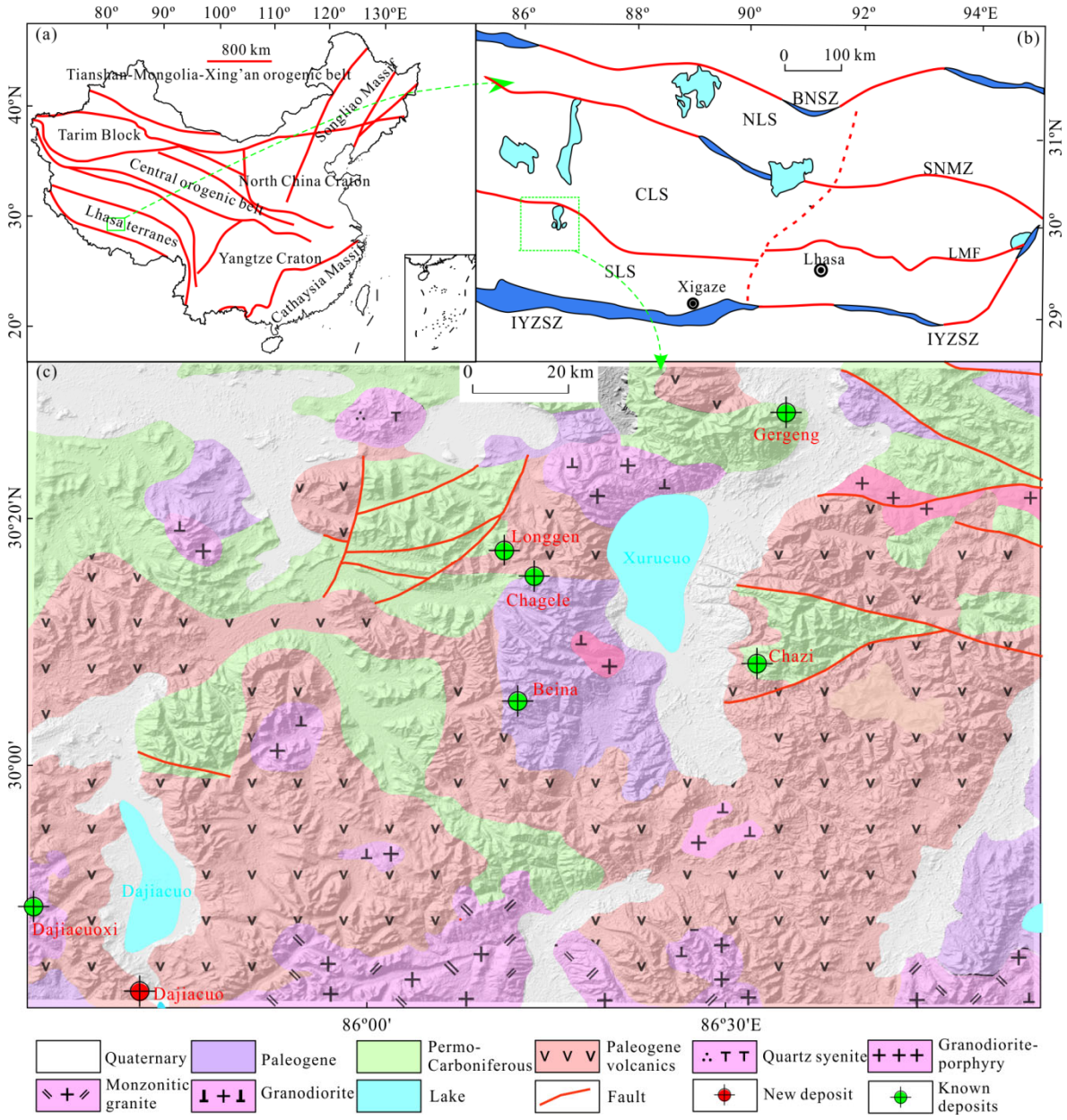

Figure 1. (a) Simplified structural map of China (No. GS(2016)2928); (b) tectonic framework in the Lhasa terrane (modified from Hou et al., 2015; Zhu et al., 2011); (c) simplified geological map of the study area. IYZSZ. India-Yarlung Zangbo suture zone; BNSZ. Bangong-Nujiang suture zone; SNMZ. Shiquanhe-Namucuo opiolitic melange belt; LMF. Lobadui-Milashan fault zone; NLS. North Lhasa subterrane; CLS. central Lhasa subterrane; SLS. southern Lhasa subterrane.

analytical technology and the effective stream sediment data processing method to discover the Dajiacuo Ag-Pb-Zn deposit, aiming to provide a convenient, fast, and efficient prospecting method for western Tibet and other areas with poor and harsh working environments.

1 STUDY AREA AND DATA

1.1 Geological Setting

The study area is located between the central Lhasa subterrane (CLS) and the southern Lhasa subterrane (SLS), which are separated by the Luobadui-Milashan fault zone (LMFZ) in southwestern Tibet (Figs. 1a–1b; Pan et al., 2006). There is an unconformable contact with Permian–Carboniferous metamorphic sedimentary rocks and Paleogene volcano-sedimentary rocks (Li et al., 2019; Zhang et al., 2018; Zhu et al., 2011). The structures are primarily EW-oriented faults of different scales and sequences, followed by genetically related NE-trending and NNW-trending faults, and a few NS-oriented faults (Fig. 1c). The exposed intrusions are mainly quartz syenite, granodiorite porphyry, monzonitic granite, and granodiorite, with zircon U-Pb ages ranging from 61–72 Ma (Liu et al., 2019; Zhang et al., 2017; Duan et al., 2014; Gao et al., 2012; Wang et al., 2012). These intrusions and the Paleogene volcanics (Fig. 1c) are closely spatially and genetically related to the known mineral deposits (Beina Pb-Zn-Ag deposit, Longgen Pb-Zn-Ag deposit, Chagele Pb-Zn-Ag-Cu deposit, Chazi Pb-Zn deposit, Gergeng Pb-Zn deposit, Dajiacuoxi Pb-Zn deposit) (Fig. 1c; Jiang et al., 2019; Liu et al., 2019; Zhang Y C et al., 2018; Zhang S Z et al., 2017; Gao et al., 2012).

1.2 Data Sources

The regional stream sediment geochemical dataset consisted of 758 stream sediment samples (Fig. 2) and 39 major and minor trace elements were analyzed at a density of one sample per 15 km^2. Detection limits and analytical methods for each of the 39 elements are shown in Table 1.

The DEM dataset was downloaded from publicly available data on the Geospatial Data Cloud Site, the Chinese Academy of Sciences (http://www.gscloud.cn). This dataset was processed using ASTER GDEM first edition (V1) and divided into four image files with a global spatial resolution of 30 m.

1.3 Geochemical Parameters and Distribution Statistics

Geochemical statistical parameters like the skewness of the original dataset revealed the non-normal distribution of all 39 elements, especially Ag, Pb, Zn, Cu, Hg, and Au (Table 2). Based on the types of mineral combinations in the Ag-Pb-Zn deposit in the study area, Ag, Pb, Zn, and Cd were selected to generate logarithmic transformation histograms and Q-Q diagrams. The histograms showed an approximately log-normal distribution pattern (Fig. 3). However, the Q-Q plots revealed the existence of multiple populations in the single dataset (Fig. 4), indicating the presence of mixed origins due to the impact of complex geological processes (Zuo et al., 2011, 2009). They also clarified that these elements did not obey the central limit theorem in their spatial distributions, and element dispersion and enrichment may have had some singularity in space.

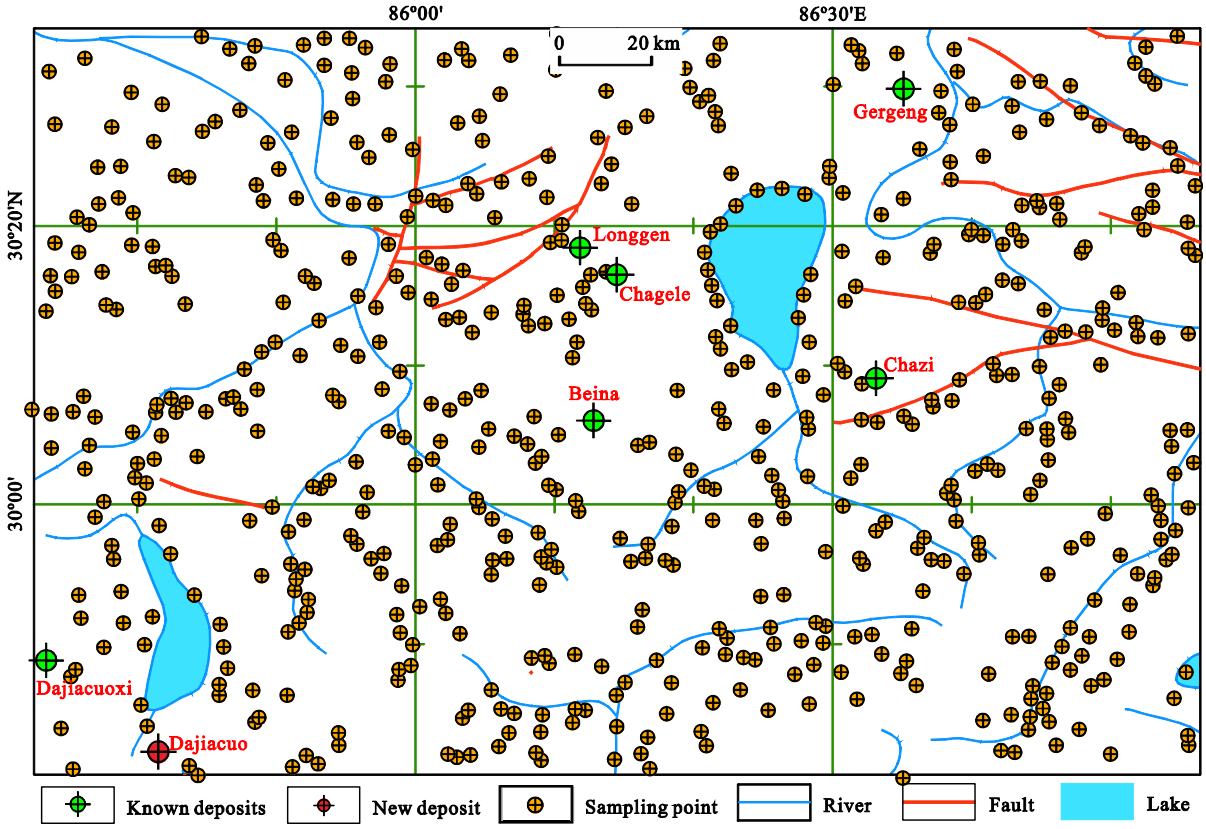

Figure 2. Stream-sediment sample location map.

Table 1 The detection limits and analytical methods of 39 elements (partially quoted Wang et al., 2011; Xie et al., 2008)

Element	Detection limit	Analytical method	Element	Detection limit	Analytical method	Element	Detection limit	Analytical method
Ag	20	ES	La	18	ICP-MS	U	0.5	ICP-MS
As	1	HG-AFS	Li	5	ICP-AES	V	5	ICP-AES
Au	0.2	GF-AAS	Mn	30	ICP-AES	W	0.5	ICP-MS
B	5	ES	Mo	0.2	ICP-MS	Y	1	XRF
Ba	50	ICP-AES	Nb	5	ICP-MS	Zn	10	ICP-AES
Be	0.5	ICP-AES	Ni	2	ICP-AES	Zr	10	XRF
Bi	0.05	ICP-MS	P	100	XRF	SiO_2	0.10 wt.%	XRF
Cd	30	ICP-MS	Pb	2	ICP-MS	Al_2O_3	0.10 wt.%	XRF
Co	1	ICP-MS	Sb	0.1	HG-AFS	TFe_2O_3	0.05 wt.%	XRF
Cr	5	XRF	Sn	1	ES	MgO	0.05 wt.%	ICP-AES
Cu	1	ICP-MS	Sr	5	ICP-AES	CaO	0.05 wt.%	ICP-AES
F	100	ISE	Th	4	ICP-MS	Na_2O	0.05 wt.%	ICP-AES
Hg	0.5	CV-AFS	Ti	100	XRF	K_2O	0.05 wt.%	XRF

Note: the units of Ag, Au, Cd, and Hg are ppb, and the units of other elements are ppm, apart from oxides (wt.%). ES. Emission spectrometry; HG-AFS. hydride generation-atomic fluorescence spectrometry; GF-AAS. graphite furnace atomic absorption spectrometry; CV-AFS. cold vapor atomic fluorescence spectrometry; ISE. ion-selective electrode; ICP-MS. inductively coupled plasma mass spectrometer; XRF. X-ray fluorescence; ICP-AES. inductively coupled plasma atomic emission spectroscopy.

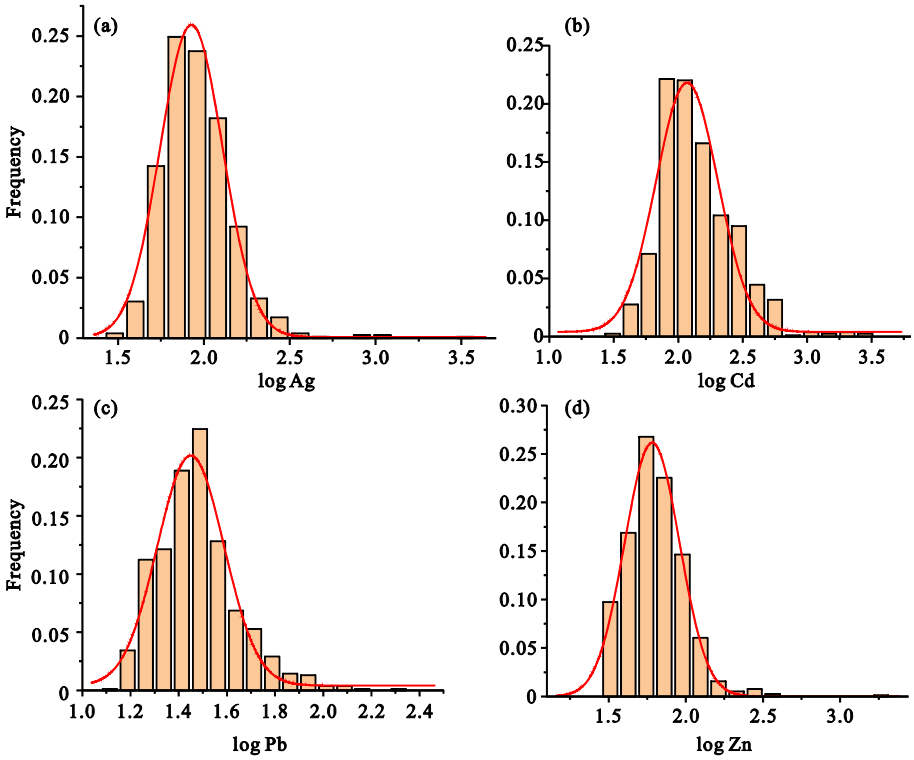

Figure 3. Histograms of (a) log Ag, (b) log Cd, (c) log Pb, and (d) log Zn.

2 METHODS

2.1 Staged Factor Analysis (SFA) and Logistic Function

As applied in the current investigation, the general procedure for SFA consisted of two main phases: the first phase involved extracting 'clean' factors and the second phase extracted the remarkable multi-element anomalous signature for mineralization to calculate reasonable factor scores (FSs) and loadings (Yousefi et al., 2014). Each of the main SFA phases was divided into sub-phases (called stages) depending on the geochemical dataset feature and type of known mineral deposits (Yousefi, 2017; Yousefi et al., 2014). To avoid significant bias in multivariate statistical analysis (e.g., SFA), we performed an ilr-transformation on the dataset (Chen et al., 2018, 2016; Yousefi et al., 2014). In addition, the ilr-transformation dataset was tested using the Kaiser-Meyer-Olkin (KMO>0.7). Test and significance of Bartlett's test of sphericity (Sig. <0.01) to de-

termine its factorability (Kaiser and Rice, 1974). Then we used SFA until the third stage (Table 3) to extract remarkable multi-element anomalous geochemical signatures for Ag-Pb-Zn deposits using Geochem Studio software (Gao et al., 2016). To improve the interpretability of the data, we retained factors with eigenvalues >1 and used thresholds with loadings higher than 0.6 (Treiblmaier and Filzmoser, 2010; van Helvoort et al., 2005). Hence, the factors were regarded as 'clean' factors, and the elements (threshold value ≤0.6) were 'noisy' elements in the 'clean' factors (Yousefi et al., 2014).

A logistic function can be used to transform boundless *FS*s into values in the range [0, 1]. In recent logistic function

Table 2 Descriptive statistics for original stream sediment geochemical data

Element	N	Minimum	Maximum	Mean	Standard deviation	Skewness	Kurtosis
Ag	758	28	3 600	107.39	149.51	17.93	399.36
As	758	1.64	218.94	23.26	20.78	3.92	22.3
Au	758	0.27	59.2	1.02	2.15	26.06	703.91
B	758	6.3	233.3	40.11	18.33	2.85	19.44
Ba	758	131.15	1 278	512.56	129.52	2.11	10.92
Be	758	1.52	16.12	3.05	1.42	5.48	36.33
Bi	758	0.09	8.32	0.45	0.43	9.93	154.35
Cd	758	30	2 470	183.67	221.68	6.41	54.23
Co	758	1.6	22.07	6.28	2.59	1.89	6.85
Cr	758	4.22	221.96	25.82	19.51	5.16	44.78
Cu	758	2.18	292.48	12.18	15.08	13.94	236.34
F	758	189.75	1 569.11	468.9	173.83	2.26	8.11
Hg	758	1	1 440	16.42	54.73	23.58	607.51
La	758	17.93	92.28	33.92	7.93	1.13	4.86
Li	758	14.94	101.93	43.49	14.47	1.58	3.26
Mn	758	112.19	2 291	456.82	249.63	2.79	11.92
Mo	758	0.2	6.54	0.8	0.76	4.2	22.28
Nb	758	5.71	28.8	12.92	3.19	0.53	1.43
Ni	758	2.89	140.49	13.76	11.28	7.33	76.76
P	758	134.5	1 465	397.44	168.45	2.53	10.4
Pb	758	13.71	8 881	44.47	321.82	27.42	753.87
Sb	758	0.1	10.71	0.95	0.76	6.75	73.36
Sn	758	0.55	22.82	3.5	2.46	3.55	18.09
Sr	758	48.58	698.77	159.18	79.52	2.56	10.22
Th	758	4.02	73.26	15.86	8.57	3.36	16.53
Ti	758	672.09	5 089.42	2 106.49	654.74	0.71	0.66
U	758	1.02	191.3	5.36	14.74	9.83	103.07
V	758	8.77	132.06	39.63	17.52	1.1	2.2
W	758	1.06	28.54	3.77	2.7	4.09	21.11
Y	758	1.91	1.91	1.91	0		
Zn	758	29.01	1 667	72.19	69.08	16.82	377.1
Zr	758	69.61	568.91	208.17	68.59	0.75	1.76
Al_2O_3	758	5.62	17.24	12.12	1.27	0.1	1.63
CaO	758	0.2	23.77	1.09	1.47	8.31	97.82
Fe_2O_3	758	0.9	7.14	2.76	0.85	1.12	2.14
K_2O	758	1.73	6.4	3.61	0.57	1.23	5.99
MgO	758	0.13	4.18	0.74	0.44	2.99	15.39
Na_2O	758	0.19	3.96	1.87	0.51	0.15	1.32
SiO_2	758	34.45	86.67	74.96	4.69	-1.98	10.99

Note: The units of Ag, Au, Cd, and Hg are ppb and the units of other elements are ppm, apart from oxides (wt.%).

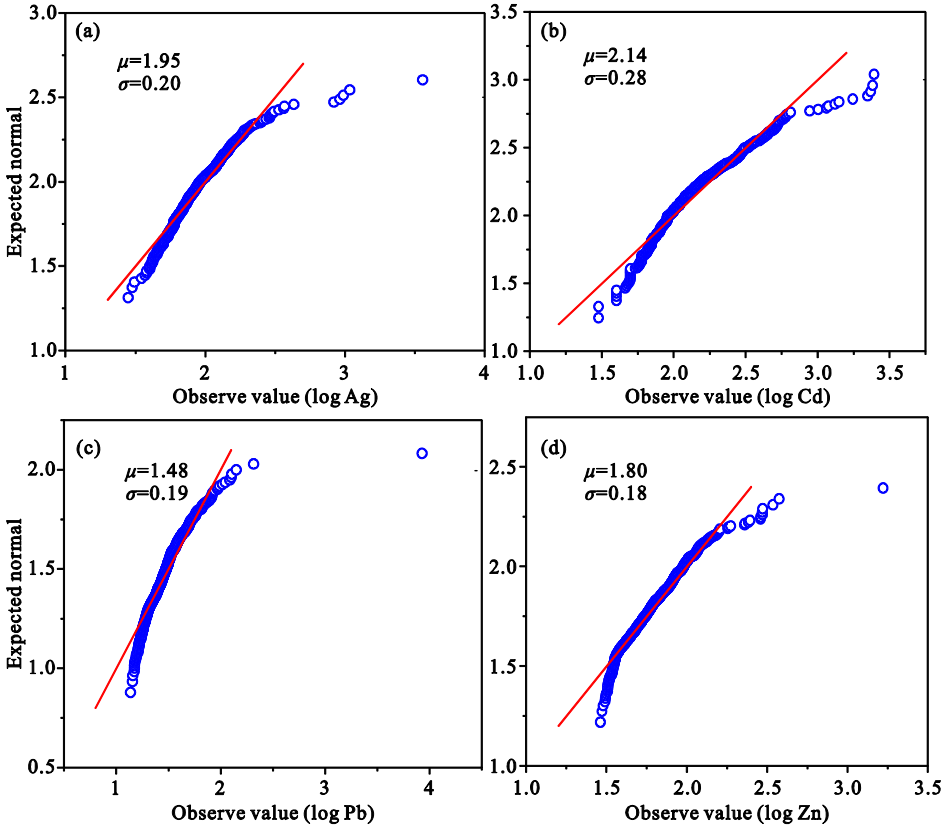

Figure 4. Q-Q plots of (a) log Ag, (b) log Cd, (c) log Pb, and (d) log Zn.

association studies, this was called the geochemical mineralization probability index (GMPI) to eliminate the negative impact on the fractal model and obtain fuzzy weights for geochemical mapping (Yousefi et al., 2014). To convert the FS values into geochemical mineralization prospectivity indices (GMPI) in the range of 0 and 1, we applied the following logistic function (Yousefi et al., 2015, 2012)

$$GMPI = \frac{e^{FS}}{1+e^{FS}} \tag{1}$$

where FS is the factor score of each sample obtained from the SFA. Thus, based on the third stage factor one (TSF1, Ag-Cd-Pb-Zn) acquired by third stage factor analysis (TSFA), the GMPI value for each geochemical sample was

$$GMPI_{\text{ore-related}} = \frac{e^{FS_{\text{Ag-Cd-Pb-Zn}}}}{1+e^{FS_{\text{Ag-Cd-Pb-Zn}}}} \tag{2}$$

where $FS_{\text{Ag-Cd-Pb-Zn}}$ is a factor score describing a multi-element ore-bearing indicator in the study area. Non-linear transformation of TSF1 into the range of 0 and 1 using the logistic function (Eq. (2); Yousefi et al., 2014) has resulted in stronger discrimination between anomalous and background values.

2.2 S-A Fractal Model and Multifractal Inverse Distance Weighting (MIDW)

S-A fractal model is a generalization of the concentration-area fractal model (C-A) applying a Fourier Transform to the frequency domain to achieve the separation of background and anomalies (Cheng, 1999). Anomalies are varied, and their intensity, size, and background values are also diverse, which can be determined by self-similarity routines in the frequency domain (Cheng, 2004, 2000). Based on self-similarity routines (Cheng, 2004), the "spectral energy density-area" (S-A) fractal model of multifractal fields was established

$$A(\geq S) \propto S^{-\beta} \tag{3}$$

where $A(\geq S)$ represents the area that exceeds the threshold of spectral energy density, $\propto$ represents the proportion, and β is the fractal dimension. The power-law spectral energy density (S) was determined on the double logarithmic plot, according to the relationship $S=(|X(\omega)|^2)$. The scatter plot was fitted to a three-segment straight line using the least square method to find the appropriate cut-off points S_1, S_2 ($S_1<S_2$) to construct a fractal filter (Liu et al., 2020). Using this fractal filter, the combined map of geochemical elements was decomposed into three different components, namely noise, background, and anomaly (Cheng et al., 2009). These two intersections were used to define the cutoff value of the filters, with $S<S_1$ representing noise, $S>S_2$ describing the background, and $S_1<S<S_2$ representing anomalies. Filters were then determined as follows.

$$\begin{aligned} G1(\omega) &= \begin{cases} 1, S(\omega) \geq S_2 \\ 0, \text{otherwise} \end{cases} \\ G2(\omega) &= \begin{cases} 1, S_1 \leq S(\omega) \leq S_2 \\ 0, \text{otherwise} \end{cases} \end{aligned} \tag{4}$$

where $G1(\omega)$ is the background filter, and $G2(\omega)$ is the anomaly filter.

However, considering spatial correlations, the multifractal

Table 3 Rotated factor matrix for the third-stages of staged factor analysis

First main phase														Second main phase	
First stage (FSFA)					First stage (FSFA)					Second stage (SSFA)				Third stage (TSFA)	
Element	FSF1	FSF2	FSF3	FSF4	Element	FSF1	FSF2	FSF3	FSF4	Element	SSF1	SSF2	SSF3	SSF4	Element	TSF1
Ag	-0.42	**0.62**	-0.12	-0.06	Sn	0.04	0.56	0.42	-0.04	Ag	-0.44	-0.13	**-0.7**	0.01	Ag	**0.76**
As	-0.01	0.18	-0.57	0.02	Sr	-0.36	**-0.66**	**-0.67**	0.06	Be	**-0.63**	-0.19	0.38	0.16	Cd	**0.89**
Au	-0.04	-0.35	-0.07	0.06	Th	-0.36	0.33	0.06	-0.11	Cd	-0.11	0.04	**-0.8**	0.08	Pb	**0.84**
B	0.33	-0.01	-0.02	0.05	Ti	**0.90**	-0.10	0.03	-0.07	Co	**0.85**	-0.06	0.08	0.04	Zn	**0.90**
Ba	-0.54	0.01	-0.01	-0.05	U	-0.41	0.00	-0.01	-0.06	Cr	**0.84**	-0.03	0.10	-0.04	Eigenvalue	2.87
Be	**-0.64**	-0.34	-0.08	0.00	V	**0.90**	-0.10	0.03	-0.07	La	-0.30	**0.71**	0.22	0.00	Var.%	71.8
Bi	0.03	0.55	-0.04	0.00	W	-0.26	0.02	0.01	-0.04	Nb	-0.21	**0.84**	0.00	0.21	Cum. Var.%	71.8
Cd	0.03	**0.82**	-0.16	0.01	Y	-0.57	-0.14	0.07	-0.60	Ni	**0.89**	-0.11	0.03	0.02	KMO	**0.75**
Co	**0.84**	-0.09	0.03	-0.07	Zn	0.03	**0.82**	-0.16	0.01	Pb	-0.24	0.15	**-0.7**	0.13	Bartlett	**0.00**
Cr	**0.83**	-0.07	0.02	0.02	Zr	0.07	0.44	**0.67**	-0.09	Sr	-0.36	**-0.68**	0.29	-0.15		
Cu	0.57	0.50	-0.03	0.05	Al_2O_3	-0.33	0.27	0.10	**-0.72**	Ti	**0.88**	0.12	0.17	0.14		
F	-0.28	0.27	0.06	-0.09	CaO	0.05	-0.26	-0.20	**0.86**	V	**0.93**	-0.10	0.19	0.01		
Hg	0.34	-0.01	-0.02	0.05	Fe_2O_3	**0.78**	0.38	0.03	0.02	Zn	0.06	0.26	**-0.9**	0.19		
La	-0.33	-0.03	**0.65**	-0.10	K_2O	-0.60	0.43	0.01	-0.10	Zr	0.06	**0.81**	-0.09	0.18		
Li	-0.52	-0.02	-0.01	-0.05	MgO	**0.76**	0.03	-0.04	0.41	Al_2O_3	-0.29	0.37	-0.24	**0.76**		
Mn	0.04	0.40	0.08	-0.07	Na_2O	-0.48	-0.42	-0.02	-0.03	CaO	-0.01	-0.24	0.16	**-0.92**		
Mo	-0.27	0.33	0.07	-0.10	Eigenvalue	9.02	5.73	2.68	1.42	Fe_2O_3	**0.79**	0.30	-0.28	-0.01		
Nb	-0.29	0.40	**0.72**	-0.15	Var.%	23.75	15.09	7.05	3.74	MgO	**0.80**	-0.02	0.02	-0.41		
Ni	**0.86**	-0.09	0.03	-0.07	Cum. Var.%	23.75	38.84	45.89	49.63	Eigenvalue	6.30	4.11	2.34	1.15		
P	0.48	0.01	0.01	0.05	KMO	**0.77**	Bartlett	**0.00**		Var.%	35.03	22.86	13.00	6.38		
Pb	-0.28	**0.74**	-0.12	-0.04						Cum. Var.%	35.03	57.88	70.89	77.26		
Sb	-0.01	0.15	-0.48	0.02						KMO	**0.80**	Bartlett	**0.00**			

Note: Loadings in bold represent the selected elements based on a threshold of 0.6 (the absolute threshold value) for each stage. KMO. Kaiser-Meyer-Olkin measure of sampling adequacy; Bartlett. significance of Bartlett's test of sphericity.

inverse distance weighting (MIDW) method (Cheng, 2000) incorporates a local singularity into the moving average interpolation model. Compared with the traditional moving average interpolation methods, the MIDW process has the advantages of improving interpolation accuracy and retaining the local structure of the interpolation surface (Zuo, 2011; Cheng, 2000, 1999). Because of these advantages, MIDW is more suitable for the interpolation of S-A fractal model than other interpolation methods. Anomalies and background from the S-A method could be calculated using the GeoDAS software system (Cheng, 2000, 1999).

2.3 Portable X-Ray Fluorescence Analysis

In this study, the instrument used for detecting the trace element contents of samples was a Niton XL3t Goldd (Thermo Fisher Scientific). During the test, the system automatically corrected instrument parameters after a certain period to ensure the accuracy of the data (Lemière, 2018). Depending on the sample type being analyzed, three test modes (mining mode, soil mode, and all-around mode) can be adopted. The mining model is appropriate for analyzing elements of higher concentrations (element content >0.2%–0.5%), the soil mode is suitable for minor and trace elements, and the all-around mode obtains comprehensive results faster than other modes (Burley et al., 2019). In this study, the all-around model was used to test the ore-related rock concentrations and improve fieldwork efficiency.

The pXRFA can effectively detect many elements (e.g., Ag, As, Cu, Cd, Pb, Sb, Zn, etc.), directly or indirectly (Druzbicka and Craw, 2013; Kovács et al., 2006). Field profile measurements of newly discovered ore-bearing rocks in the Dajiacuo region were carried out using pXRFA.

3 RESULTS AND DISCUSSION

3.1 Selection of Factors Associated with Ag-Pb-Zn Mineralization

We used SFA up to the third stage (Table 3): the first and second stages were used to remove the 'noisy' elements, and the third stage was used to extract the essential composite elements indicating geochemical anomalies (Yousefi et al., 2014). It can be seen from Table 3 that KMO values for each stage were >0.75 and Sig. were all <0.01, indicating that this dataset was suitable for factor analysis. For the dataset in this paper, the first stage factor one (FSF1) represented a Be-Co-Cr-Ni-Ti-V-Fe_2O_3-MgO association, FSF2 represented an Ag-Cd-Pb-Sr-Zn association, FSF3 represented a La-Nb-Sr-Zr association, and FSF4 represented an Al_2O_3-CaO association (Table 3).

Because of the existence of indicator elements (i.e., Ag, Pb, Zn, Cd, Sr), the FSF2 signature reflected the existence of Ag-Pb-Zn deposits. However, the 20 elements in the first stage factor analysis (FSFA) such as As, Au, did not contribute importantly to all factors; hence, they were not used in the second stage factor analysis (SSFA). After removing the 20 elements, the contributions of Ag, Cd, Pb, and Zn to the second stage factor three (SSF3) were enhanced in the SSFA (Table 3), and the negative correlation of Sr was eliminated. Factors SSF1, SSF2, and SSF4 (Table 3) were considered 'clean' because there were no 'noisy' elements.

A small number of extracted factors provide the best results with respect to interpretability (Reimann et al., 2002), and SSF1, SSF2, and SSF4 are not appropriate multi-element features. Therefore, even though each of these factors was positively correlated with elements that had a small positive or negative influence in the SSF3, the SSF3 would still include "noisy" elements for every sample (Yousefi et al., 2014). To further filter out geochemical noise, only elements with absolute loading values >0.6 on SSF3 were used in the third stage factor analysis (TSFA) (Table 3). In the TSFA, we obtained the combination of Ag-Cd-Pb-Zn, which means that it was related to the Ag-Pb-Zn mineralization. Hence, the third stage factor one (TSF1) was selected as a factor correlated with Ag-Pb-Zn mineralization

3.2 Separation of Background Mineral-Induced Geochemical Anomalies

A Fourier transform was used to transform the GMPI datasets into the frequency domain. The abscissa and ordinate were spectral energy density (S) and area (A), respectively, and plotted on a double logarithmic plot (Fig. 5). Three straight lines were fitted to the data, separated with the threshold values log S_1=4.33 (S_1=76.03) and log S_2=8.61 (S_2=5 511.45). The three lines defined three filters: S≤76.03 was the noise filter, 76.03≤S≤5 511.45 was the anomaly filter, and S≥5 511.45 was the background filter. The left-line represented high-frequency noise in the geochemical progress (Cheng et al., 2010). The midline indicated the middle-frequency anomaly, which is usually connected to complex geological processes and mineralization (volcanic rock and intersections of faults) that are favorable areas for Ag-Pb-Zn deposits. The right-line displayed the low-frequency background, which may have reflected beneficial rock types (Cheng et al., 2010). Anomalies and background maps for geochemical combination elements were obtained by transforming the three intervals of S from the frequency domain to the spatial domain using the inverse Fourier transform (Figs. 6a–6b).

The anomalies map shows that high-value areas (close to red) appear to have SE-NW trend (main) and NE-SW trend (subordinate), and occurred around intrusions and along SE-NW trending faults, or intersections of faults (Fig. 6b). They were favorable areas for the formation, preservation, and

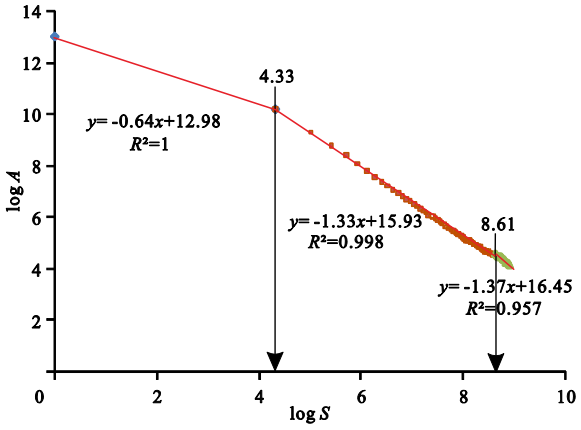

Figure 5. Natural log-log of the relationship between spectral energy density and area.

prospecting of ore deposits and indicated the potential for the discovery of Ag-Pb-Zn deposits in the study area. However, the high-value areas (near red) in the background map had an E-W trend and were mainly located in the middle of the study area (Fig. 6a). The high-value regions were firmly related to volcanic rocks and intrusions, which suggested a source of Ag-Cd-Pb-Zn in the region. The S-A method not only effectively narrowed the exploration area (Zuo, 2014, 2011) but also separated the mineralization-derived geochemical anomalies from the background.

3.3 Establishment of DEM-Based Geochemical Models (DGM) to Identify Anomaly Sources

In the attempt of any exploration target, the exploration scale and the corresponding metallogenic sub-system must be determined. For this reason, the ore-forming process is divided into three sub-systems: pre- syn-, and post-mineralization sub-systems, which is helpful to better understand their operation

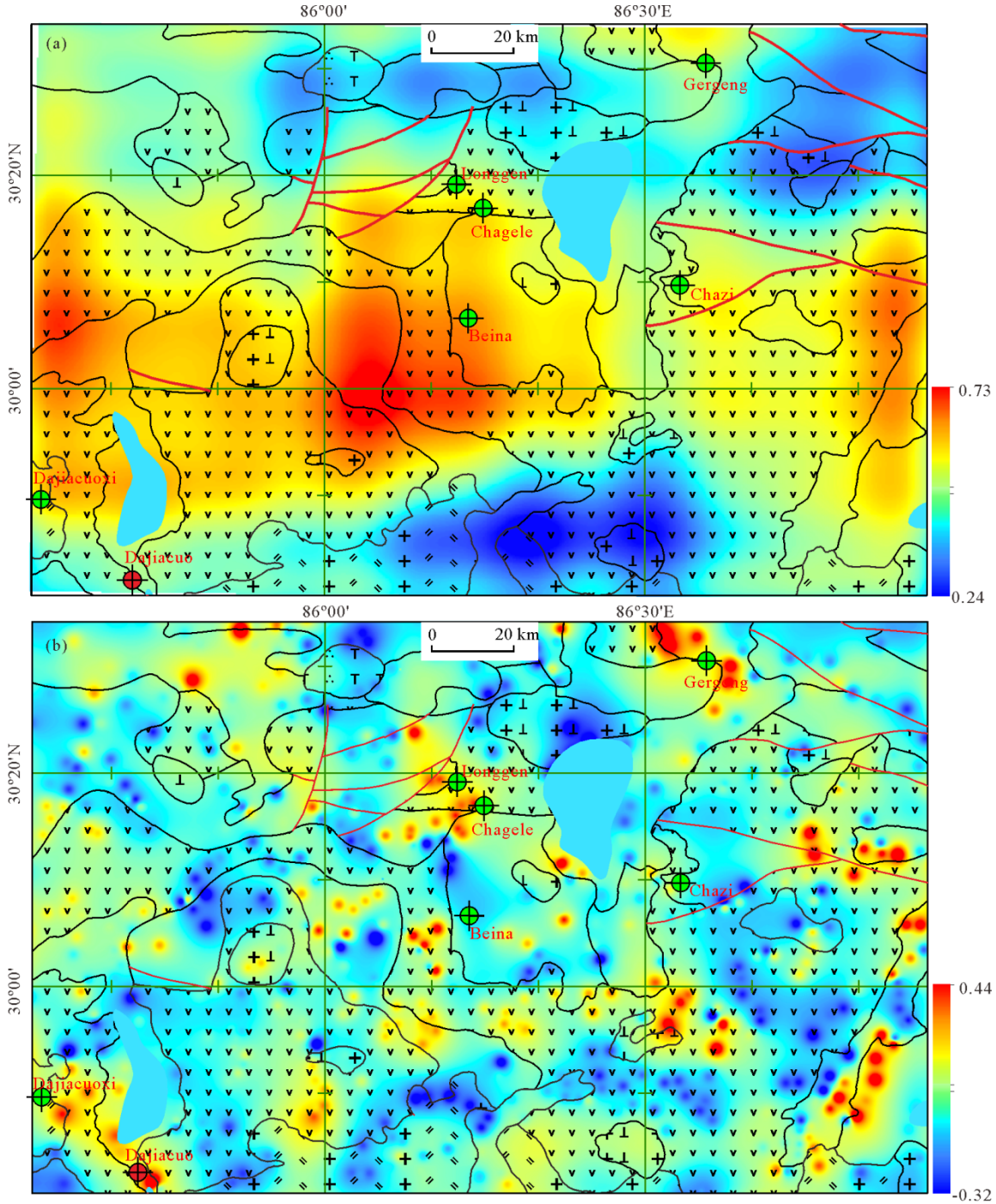

Figure 6. Geochemical background (a) and anomalies (b) map of GMPI in the study area, compiled using the spectrum-area model. Dajiacuo: Ag-Pb-Zn deposit; Dajiacuoxi: Pb-Zn deposit; Beina: Pb-Zn-Ag deposit; Chagele: Pb-Zn-Ag-Cu deposit; Longgen: Pb-Zn-Ag deposit; Chazi: Pb-Zn deposit; Gergeng: Pb-Zn deposit.

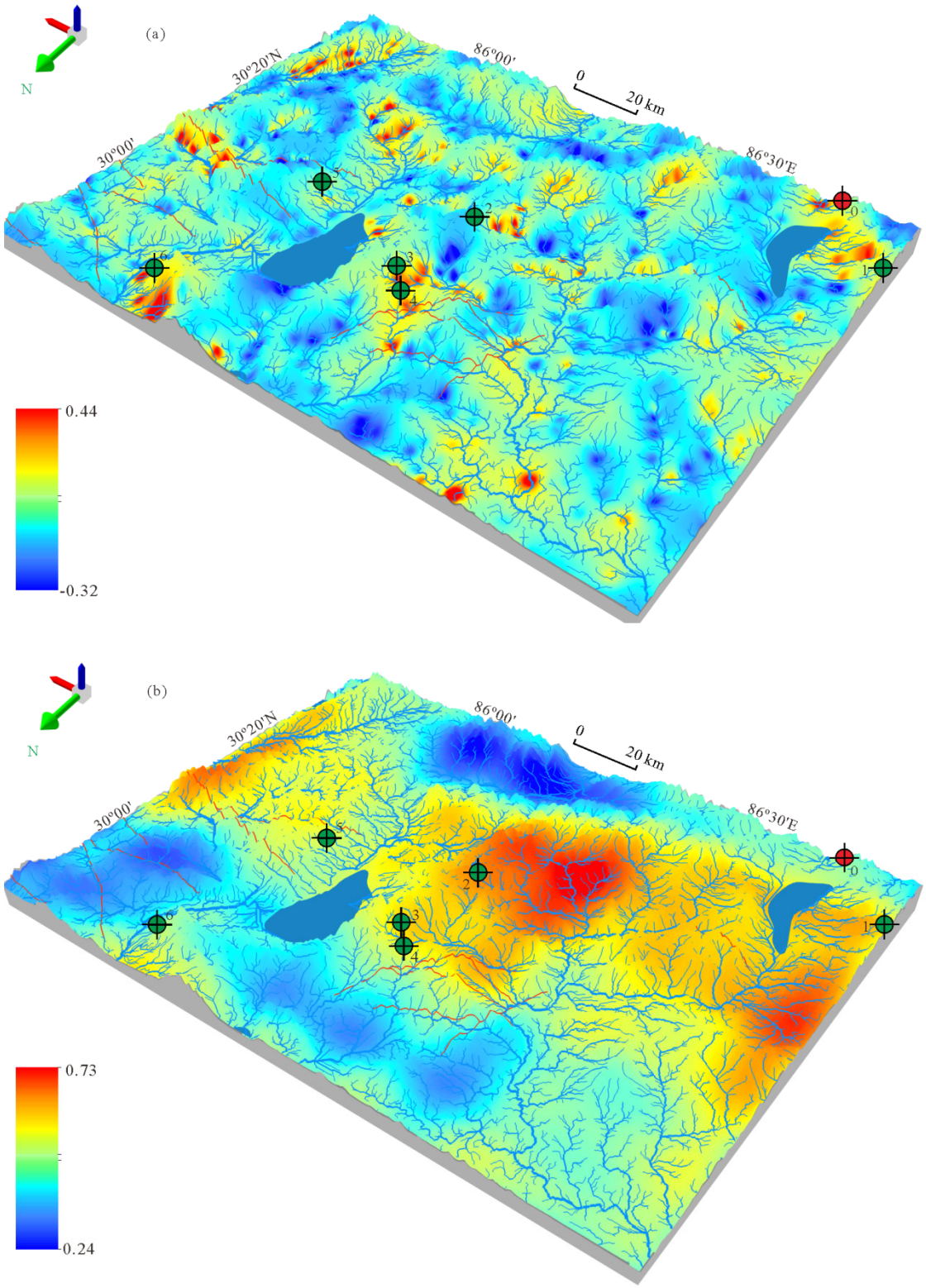

Figure 7. DEM-based geochemical model (DGM). (a) Geochemical anomalies and (b) geochemical background map of the study area. 0. Dajiacuo Ag-Pb-Zn deposit; 1. Dajiacuoxi Pb-Zn deposit; 2. Beina Pb-Zn-Ag deposit; 3. Chagele Pb-Zn-Ag-Cu deposit; 4. Longgen Pb-Zn-Ag deposit; 5. Chazi Pb-Zn deposit; 6. Gergeng Pb-Zn deposit.

mode at different scales (Yousefi et al., 2019). However, the relative importance of these three subsystems depends on the scale of key ore-forming geological processes, and the improper combination of relevant target standards of different sizes will inevitably lead to biased and ineffective target exploration models (Yousefi et al., 2019). Therefore, the exploration targets from regional to deposit scale are outcrop mineralization, partial outcrop mineralization, concealed orebody and blind orebody in each subsystem. Based on the sampling density and the phenomenon of oxidation and secondary geochemical element

diffusion under superficial conditions, it is inferred that the stream sediments involved in this paper belong to the regional scale and the post-mineralization sub-systems. Therefore, according to the modeling idea of the exploration information system, the measurement of the stream sediments can achieve the purpose of pointing to the potential deposit location (outcrop mineralization) (Yousefi et al., 2019, 2013, 2012).

Figures 7a and 7b show the geochemical patterns identified by the S-A model, which are believed to be related to mineralization, on the DEM and drainage distribution map from ArcGIS10.2 software.

From the DGM, it appeared that the anomaly to the east of the Dajiacuoxi (No. 1) deposit was generated by mineralization. An anomalous area also exists to the west of the Beina (No. 2) deposit, which appeared to originate from it at a higher elevation, but the area was relatively small. Chagele (No. 3) and Longgen (No. 4) Deposits were the two most significant deposits in the study area, with Pb-Zn reserves of more than 1.1 million tons (Zhang et al., 2018; Gao et al., 2012). Therefore, the area of geochemically anomalous responses to the two deposits was more extensive than that of other deposits. The anomalous area to the east of the Gergeng (No. 6) deposit was presumed to be a geochemical halo produced by weathering and leaching of the deposit. At the same time, the anomaly to the north was not its down-drainage, as indicated by the DGM.

However, none of the deposits in the study area were located in the center of the geochemical anomalous halo. Due to the critical influence of topography and drainage, the elements migrated under supergene conditions. The flow rate of water increased as relief increased, and weathering and denudation also accelerated, which was conducive to the migration of elements (Fig. 8). The downstream dilution of stream sediment anomalies was derived from the erosion and dissolution of water (Jiang et al., 2006; Hawkes 1976; Figs. 8a–8b). Steep terrain is prone to landslides and collapse, resulting in the displacement of an anomaly from its source (Zhang 2007; Figs. 8c–8d). Furthermore, the elements Ag, Cd, Pb, and Zn are chalcophile elements, and their chemical properties are very similar (Goldschmidt, 1937). Cadmium is generally present in sphalerite in the form of isomorphism, and silver is present in galena in the form of isomorphism or mechanical mixing (Levinson, 1980). According to the DGM and the migration behavior of the elements Ag, Cd, Pb, and Zn, we speculate that it was likely that there was an Ag-Pb-Zn deposit in the Dajiacuo region (Fig. 9). The DGM not only intuitively produces three-dimensional (3D) visualization of anomalies and backgrounds (Zuo et al., 2016), but also provides an excellent method to identify sources of anomalies.

3.4 Verification of Anomalies Using pXRFA

According to the geochemical anomalies in the Dajiacuo region, we measured the cross-section of the mineralized zone at intervals of about 50 m (Fig. 9). pXRFA was used to analyze samples along two transects, with measurements taken at intervals of approximately 50 m. The first transect (PM01) consisted of 14 points and the second (PM02) had 35 points (Fig. 10). One of the applications of this method is to measure ore grade with reliable accuracy (Lemière, 2018; Bosco, 2013). The statistical parameters for the grade values of the samples measured by pXRFA are shown in Table 4.

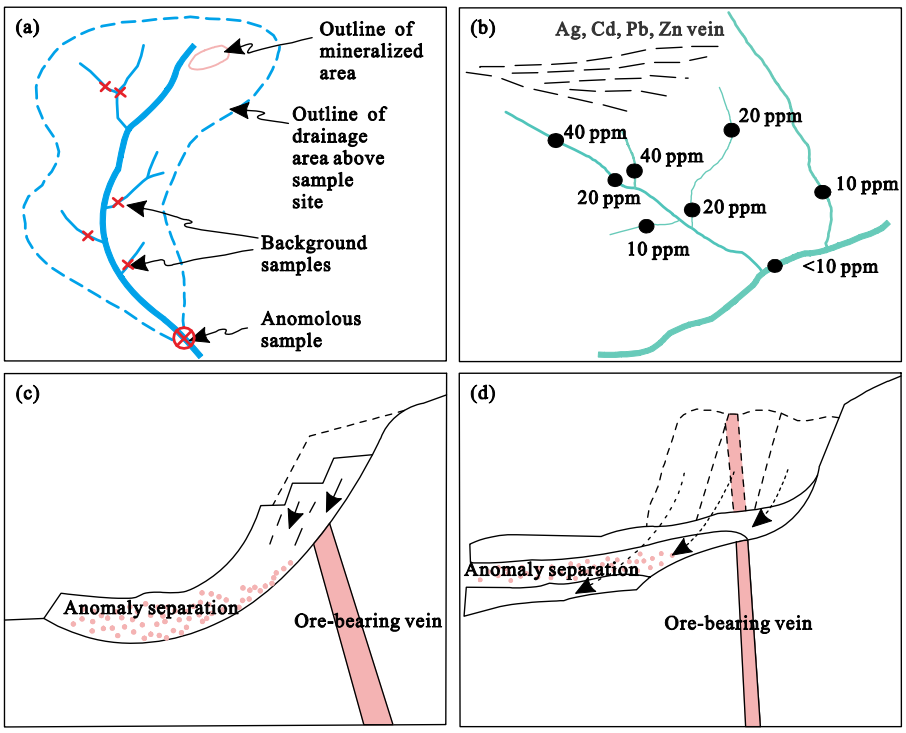

Figure 8. Schematic diagram of dispersion from mineralization. (a) Definition of drainage parameters. (b) The downstream dilution of stream sediment anomalies. (c) Separation anomaly caused by the landslide. (d) Buried halo formed by collapse. The dashed and solid lines represent the state before and after the collapse and landslide, respectively, in (c) and (d).

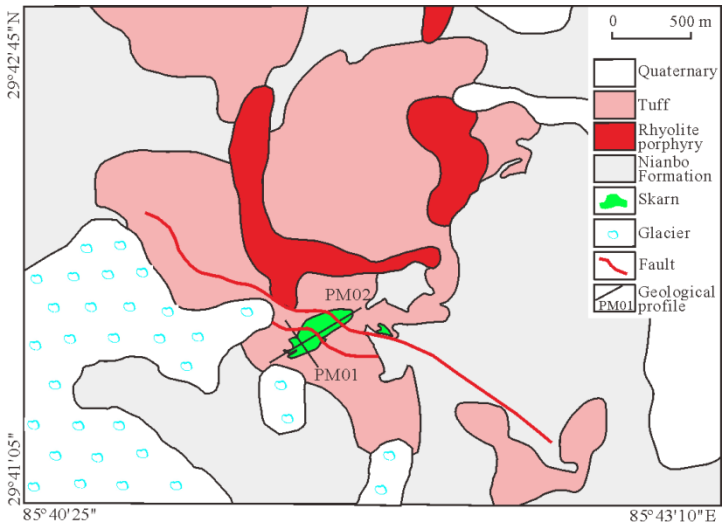

Figure 9. Geological map of the Dajiacuo region.

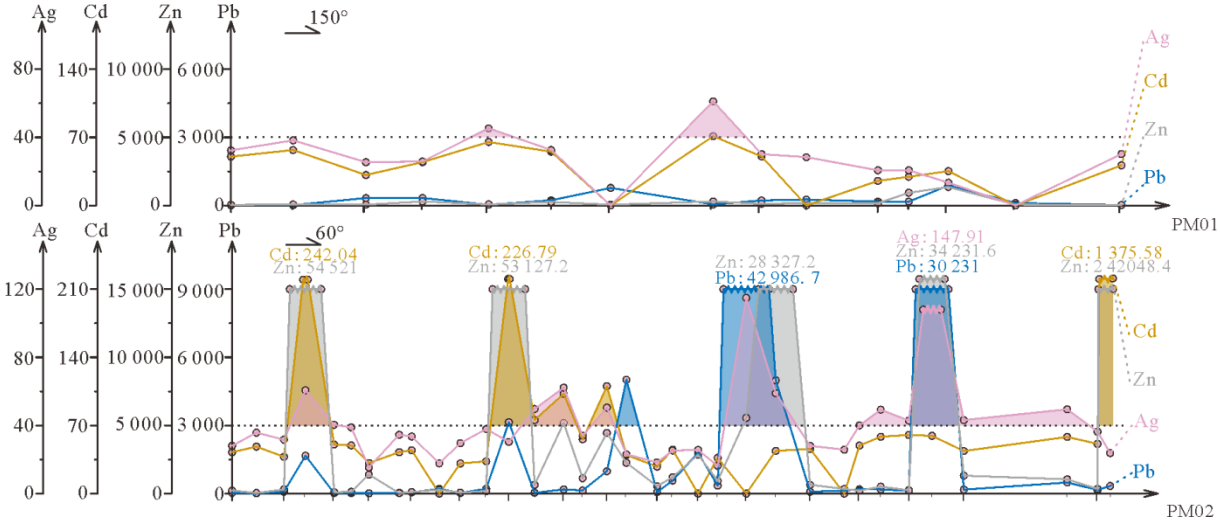

Figure 10. Section diagrams of element grades of Ag, Cd, Pb and Zn on sections 1 (PM01) and 2 (PM02) at Dajiacuo using pXRFA.

Table 4 Statistical parameters for the grades in the Dajiacuo region.

Element	Cutoff grade	Highest grade	The arithmetic mean of exceeding the cutoff grade
Ag	40 ppm	147.9 ppm	62.6 ppm
Pb	0.30 wt.%	4.20 wt.%	1.70 wt.%
Zn	0.50 wt.%	24.20 wt.%	6.00 wt.%

The highest grades of Pb and Zn were found at the center of the mineralized zone, and Ag also showed a good relationship with Pb and Zn in the profile. The principal host minerals for Pb and Zn are galena and sphalerite, respectively, which can be seen with the naked eye. However, it is challenging to identify scarce ore minerals such as argentite in the field. Argentite is easily hosted in the galena crystal lattice, which can be identified by pXRFA (Fig. 10). With the assistance of the pXRFA, we verified the presence of Ag, Pb, and Zn above the cutoff grades in the anomalous area.

The new exploration was used to verify that the geochemical anomaly area of Dajiacuo (No. 0) (Fig. 7b) is a newly discovered deposit in the southwestern part of the study area. The skarn mineralization alteration zone (length: 500 m, width: 300 m) hosting Pb-Zn mineralization (length: 200 m, width: 100 m) was found successfully, and the skarn and the NW-trending faults strictly controlled mineralization. The alteration characteristics showed strong skarnization and epidotization (Figs. 11a–11b), and the mineralization consisted of galena and sphalerite (Figs. 11e–11f), accompanied by malachite and pyrite (Figs. 11c–11d).

4 CONCLUSIONS

In this paper, spectrum-area fractal modeling and pXRFA (portable X-ray fluorescence analysis) were used to identify and verify anomalies potentially related to mineralization. The

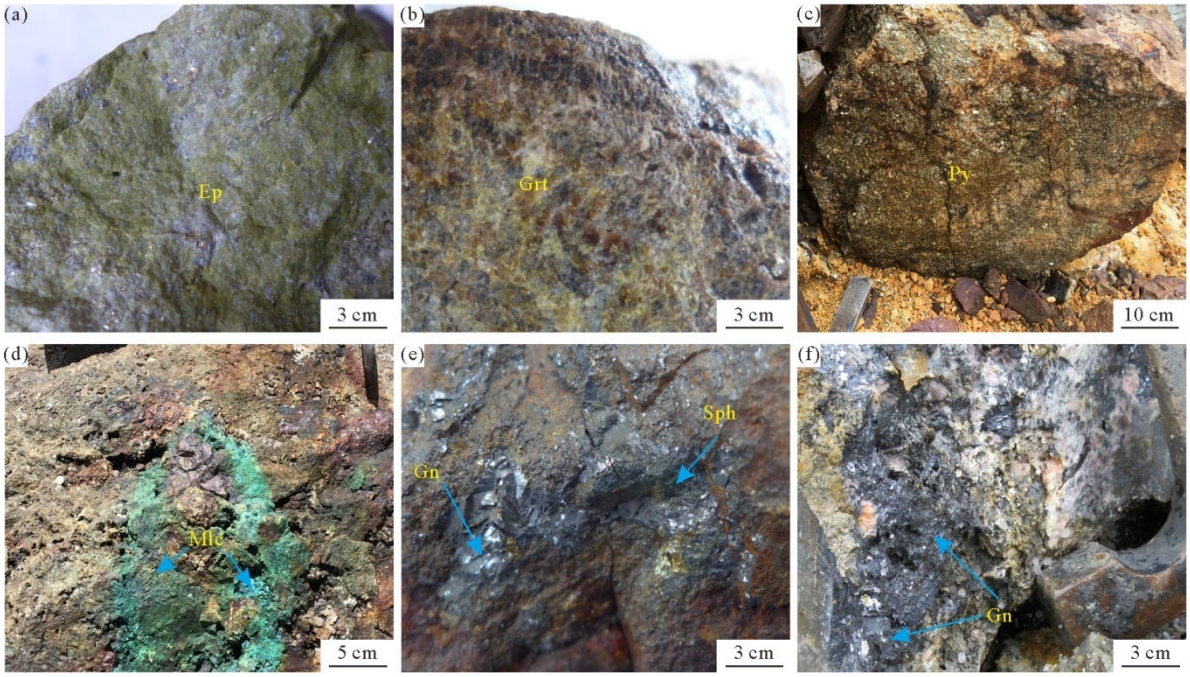

Figure 11. Representative photographs of rocks from geochemically anomalous areas in the Dajiacuo deposit. (a) Epidote skarn; (b) garnet skarn; (c) massive pyrite hosted in tuff; (d) malachite staining on epidote skarn; (e), (f) sphalerite and galena hosted in the tuff. Mineral symbols: Grt. garnet; Ep. epidote; Mlc. malachite; Gn. galena; Sph. sphalerite; Py. pyrite.

following conclusions can be drawn from this study.

(1) The hybrid SFA and S-A multifractal modeling method is a beneficial tool for identifying geochemical anomalies. The former was used to accurately verify the Pb-Zn-Ag-Cd geochemical compositional assemblages, and the latter successfully identified geochemical anomalies and background values associated with Ag-Pb-Zn mineralization in Dajiacuo-Xurucuo, Tibet.

(2) The Ag-Pb-Zn anomalies were associated with intrusions, volcanics, and were in the vicinity of faults, and all deposits were located along the long axis of anomalies extending to high elevation areas.

(3) The method suggested the presence of hitherto-unknown mineralization at Dajiacuo, and abundant Pb-Zn-Ag mineralization was identified by pXRFA in the source areas of the stream-sediment anomalies.

(4) The deviation between the anomalous center and the discovered deposits may have been caused by the dilution of the downstream catchment basin and the migration of elements produced by topographic relief. Hence, the spectrum-area fractal modeling and pXRFA methods provide a helpful tool for finding sources of anomalies during stream sediment geochemistry exploration.

ACKNOWLEDGMENTS

This study was funded by the Fundamental Research Funds for the Central Universities, China University of Geosciences (Wuhan) (No. 2019132) and China Geological Survey (No. DD20190159-33). We would like to thank the editors, and anonymous reviewers for their constructive and helpful reviews. We thank Prof. Dr. Renguang Zuo, Prof. Dr. Stephen Amor, who helped improve the manuscript from an earlier version of the paper. We appreciate the assistance of the staff at the Wuhan Sample Solution Analytical Technology Co., Ltd., Wuhan for their help with geochemical analyses. The final publication is available at Springer via https://doi.org/10.1007/s12583-020-1323-9.

REFERENCES CITED

Allégre, C. J., Courtillot, V., Tapponnier, P., et al., 1984. Structure and Evolution of the Himalaya-Tibet Orogenic Belt. *Nature*, 307(5946): 17–22. https://doi.org/10.1038/307017a0

Bosco, G. L., 2013. Development and Application of Portable, Hand-Held X-Ray Fluorescence Spectrometers. *Trac Trends in Analytical Chemistry*, 45: 121–134. https://doi.org/10.1016/j.trac.2013.01.006

Burley, L. L., Barnes, S. J., Laukamp, C., et al., 2019. Corrigendum to "Rapid Mineralogical and Geochemical Characterization of the Fisher East Nickel Sulphide Prospects, Western Australia, Using Hyperspectral and pXRF Data". *Ore Geology Reviews*, 109: 645. https://doi.org/10.1016/j.oregeorev.2017.04.032

Chen, X., Xu, R. K., Zheng, Y. Y., et al., 2018. Identifying Potential Au-Pb-Ag Mineralization in SE Shuangkoushan, North Qaidam, Western China: Combined Log-Ratio Approach and Singularity Mapping. *Journal of Geochemical Exploration*, 189: 109–121. https://doi.org/10.1016/j.gexplo.2017.04.001

Chen, X., Zheng, Y. Y., Xu, R. K., et al., 2016. Application of Classical Statistics and Multifractals to Delineate Au Mineralization-Related Geochemical Anomalies from Stream Sediment Data: A Case Study in Xinghai-Zeku, Qinghai, China. *Geochemistry*: *Exploration*, *Environment*, *Analysis*, 16(3/4): 253–264. https://doi.org/10.1144/geochem2016-424

Cheng, Q. M., 1999. Spatial and Scaling Modelling for Geochemical Anomaly Separation. *Journal of Geochemical Exploration*, 65(3): 175–194. https://doi.org/10.1016/s0375-6742(99)00028-x

Cheng, Q. M., 2000. GeoData Analysis System (GeoDAS) for Mineral Exploration: Unpublished User's Guide and Exercise Manual. Material

for the Training Workshop on GeoDAS, York University

Cheng, Q. M., 2004. A New Model for Quantifying Anisotropic Scale Invariance and for Decomposition of Mixing Patterns. *Mathematical Geology*, 36(3): 345–360. https://doi.org/10.1023/b:matg.0000028441.62108.8a

Cheng, Q. M., 2012. Singularity Theory and Methods for Mapping Geochemical Anomalies Caused by Buried Sources and for Predicting Undiscovered Mineral Deposits in Covered Areas. *Journal of Geochemical Exploration*, 122: 55–70. https://doi.org/10.1016/j.gexplo.2012.07.007

Cheng, Q. M., Zhang, S. Y., Zuo, R. G., et al., 2009. Progress of Multifractal Filtering Techniques and Their Applications in Geochemical Information Extraction. *Earth Science Frontiers*, 16(2): 185–198 (in Chinese with English Abstract)

Cheng, Q., Xia, Q., Li, W., et al., 2010. Density/Area Power-Law Models for Separating Multi-Scale Anomalies of Ore and Toxic Elements in Stream Sediments in Gejiu Mineral District, Yunnan Province, China. *Biogeosciences*, 7(10): 3019–3025. https://doi.org/10.5194/bg-7-3019-2010

Dewey, J. F., Burke, K. C. A., 1973. Tibetan, Variscan, and Precambrian Basement Reactivation: Products of Continental Collision. *The Journal of Geology*, 81(6): 683–692. https://doi.org/10.1086/627920

Druzbicka, J., Craw, D., 2013. Evolving Metalloid Signatures in Waters Draining from a Mined Orogenic Gold Deposit, New Zealand. *Applied Geochemistry*, 31: 251–264. https://doi.org/10.1016/j.apgeochem.2013.01.011

Duan, Z. M., Li, G. M., Li, Y. X., et al., 2014. Geochronology and Geochemical Characteristics of Ore-Bearing Porphyry in Longgen Lead-Zinc Deposit of Middle-Gangdese Metallogenic Belt, Tibet. *Mineral Deposits*, 33(3): 625–638. https://doi.org/10.3969/j.issn.0258-7106.2014.03.012 (in Chinese with English Abstract)

Gao, S. B., 2015. Copper-Iron Polymetal Metallogenesis and Exploration Direction in the Western of Gangdese Metallogenic Belt, Tibet: [Dissertation]. China University of Geosciences, Wuhan. 1–212 (in Chinese with English Abstract)

Gao, S. B., Zheng, Y. Y., Jiang, J. S., et al., 2019. Geochemistry and Geochronology of the Gebunongba Iron Polymetallic Deposit in the Gangdese Belt, Tibet. *Journal of Earth Science*, 30(2): 296–308. https://doi.org/10.1007/s12583-018-0984-0

Gao, S. B., Zheng, Y. Y., Tian, L. M., et al., 2012. Geochronology of Magmatic Intrusions and Mineralization of Chagele Copper-Lead-Zinc Deposit in Tibet and Its Implications. *Earth Science*, 37(3): 507–514. https://doi.org/10.3799/dqkx.2012.057 (in Chinese with English Abstract)

Gao, Y., Wang, L., Liu, Q., 2016. Geochem Studio Boosts Geochemical Informatization. *China Mining News*, 10: 1 (in Chinese with English Abstract)

Goldschmidt, V. M., 1937. The Principles of Distribution of Chemical Elements in Minerals and Rocks. The Seventh Hugo Müller Lecture, Delivered before the Chemical Society on March 17th, 1937. *Journal of the Chemical Society* (*Resumed*), 1: 655–673. https://doi.org/10.1039/jr9370000655

Hawkes, H. E., 1976. The Downstream Dilution of Stream Sediment Anomalies. *Journal of Geochemical Exploration*, 6(1/2): 345–358. https://doi.org/10.1016/0375-6742(76)90023-6

He, J. Z., Yao, S. Z., Zhang, Z. P., et al., 2013. Complexity and Productivity Differentiation Models of Metallogenic Indicator Elements in Rocks and Supergene Media around Daijiazhuang Pb-Zn Deposit in Dangchang County, Gansu Province. *Natural Resources Research*, 22(1): 19–36. https://doi.org/10.1007/s11053-012-9193-1

Hou, Z. Q., Duan, L. F., Lu, Y. J., et al., 2015. Lithospheric Architecture of the Lhasa Terrane and Its Control on Ore Deposits in the Himalayan-Tibetan Orogen. *Economic Geology*, 110(6): 1541–1575. https://doi.org/10.2113/econgeo.110.6.1541

Jiang, J. S., Gao, S. B., Zheng, Y. Y., et al., 2019. Sulphur and Lead Isotopic Compositions of the Pb-Zn Polymetallic Deposits in the Linzizong Volcanic Area, Gangdese Belt, Tibet: Implications for Variation Characteristics of Ore-Forming Material Sources and Exploration Targeting. *Geological Journal*, 55(1): 650–670. https://doi.org/10.1002/gj.3424

Jiang, J. Y., Cheng, J. J., Qi, S. H., et al., 2006. Applied Geochemistry. China University of Geosciences Press CO., LTD, Wuhan. 340 (in Chinese with English Abstract)

Kaiser, H. F., Rice, J., 1974. Little Jiffy, Mark IV. *Educational and Psychological Measurement*, 34(1): 111–117. https://doi.org/10.1177/00131644 7403 400115

Kang, S. C., Xu, Y. W., You, Q. L., et al., 2010. Review of Climate and Cryospheric Change in the Tibetan Plateau. *Environmental Research Letters*, 5(1): 015101. https://doi.org/10.1088/1748-9326/5/1/015101

Ke, X. Z., Xie, S. Y., Zheng, Y. Y., et al., 2015. Multifractal Analysis of Geochemical Stream Sediment Data in Bange Region, Northern Tibet. *Journal of Earth Science*, 26(3): 317–327. https://doi.org/10.1007/s12583-015-0538-7

Kovács, E., Dubbin, W. E., Tamás, J., 2006. Influence of Hydrology on Heavy Metal Speciation and Mobility in a Pb-Zn Mine Tailing. *Environmental Pollution*, 141(2): 310–320. https://doi.org/10.1016/j.envpol.2005.08.043

Lemière, B., 2018. A Review of pXRF (Field Portable X-Ray Fluorescence) Applications for Applied Geochemistry. *Journal of Geochemical Exploration*, 188: 350–363. https://doi.org/10.1016/j.gexplo.2018.02.006

Levinson, A. A., 1980. Introduction to Exploration Geochemistry. Applied Publishing, Alberta. 326

Li, W., Wu, Y. C., 2018. Analysis and Discussion on the Current Situation of Geological Exploration and Prospecting Process in Tibet. *Western Exploration Project*, 269(9): 168–169, 173 (in Chinese with English Abstract)

Li, Y., Zhang, C., Liu, X. Y., et al., 2019. Metamorphism and Oceanic Crust Exhumation—Constrained by the Jilang Eclogite and Meta-Quartzite from the Sumdo (U)HP Metamorphic Belt. *Journal of Earth Science*, 30(3): 510–524. https://doi.org/10.1007/s12583-019-0894-9

Liu, B. L., Guo, K., Li, C., et al., 2020. Copper Prospectivity in Tibet, China: Based on the Identification of Geochemical Anomalies. *Ore Geology Reviews*, 120(5): 102632. https://doi.org/10.1016/j.oregeorev.2018.07.015

Liu, J., Zheng, Y. Y., Gao, S. B., et al., 2019. Zircon U-Pb Dating, Geochemistry, and Sr-Nd-Pb-Hf Isotopes of the Subvolcanic Intrusion from Beina Pb-Zn-(Ag) Deposit in the Southern Lhasa Terrane, Tibet: Implications for Petrogenesis and Mineralization. *Geological Journal*, 54(4): 2064–2083. https://doi.org/10.1002/gj.3284

Long, Y. Z., Yang, X. Y., Yang, M., et al., 2019. Exploration and Sources of Bauxite Deposit in the Boloven Plateau, Southern Laos. *Journal of Earth Science*, 30(1): 121–130. https://doi.org/10.1007/s12583-019-0857-1

Newlander, K., Goodale, N., Jones, G. T., et al., 2015. Empirical Study of the Effect of Count Time on the Precision and Accuracy of pXRF Data. *Journal of Archaeological Science*: *Reports*, 3: 534–548. https://doi.org/10.1016/j.jasrep.2015.07.007

Pan, G. T., Mo, X. X., Hou, Z. Q., et al., 2006. The Spatial-Temporal Framework of the Gangdese Orogenic Belt and Its Evolution. *Acta Petrologica Sinica*, 22(3): 521–533 (in Chinese with English Abstract)

Reimann, C., Filzmoser, P., Garrett, R. G., 2002. Factor Analysis Applied to Regional Geochemical Data: Problems and Possibilities. *Applied Geochemistry*, 17(3): 185–206. https://doi.org/10.1016/s0883-2927(01)00066-x

Treiblmaier, H., Filzmoser, P., 2010. Exploratory Factor Analysis Revisited: How Robust Methods Support the Detection of Hidden Multivariate Data Structures in IS Research. *Information & Management*, 47(4): 197–207. https://doi.org/10.1016/j.im.2010.02.002

van Helvoort, P. J., Filzmoser, P., van Gaans, P. F. M., 2005. Sequential Factor Analysis as a New Approach to Multivariate Analysis of Heterogeneous Geochemical Datasets: An Application to a Bulk Chemical Characterization of Fluvial Deposits (Rhine-Meuse Delta, the Netherlands). *Applied Geochemistry*, 20(12): 2233–2251. https://doi.org/10.1016/j.apgeochem.2005.08.009

Wang, B. D., Guo, L., Wang, L. Q., et al., 2012. Geochronology and Petrogenesis of the Ore-Bearing Pluton in Chagele Deposit in the Middle of the Gangdese Metallogenic Belt. *Acta Petrologica Sinica*, 28(5): 1647–1662 (in Chinese with English Abstract)

Wang, H. M., Chen, S. Y., 2015. Extraction and Evaluation of Au, Pb, Zn Mineralization Information in the Dulan Area, Northern Margin of Qaidam. *Acta mineralogica Sinica*, 35 (S1): 934 (in Chinese with English Abstract)

Wang, X., Xie, X., Zhang, B., et al., 2011. Geochemical Probe into China's Continental Crust. *Acta Geoscientica Sinica*, 32(S1): 65–83 (in Chinese with English Abstract)

Xi, X., Li, M., 2012. Regional Geochemical Exploration in China: From 1999 to 2009. *Geology in China*, 39(2): 267–282 (in Chinese with English Abstract)

Xie, X. J., Wang, X. Q., Zhang, Q., et al., 2008. Multi-Scale Geochemical Mapping in China. *Geochemistry*: *Exploration*, *Environment*, *Analysis*, 8(3/4): 333–341. https://doi.org/10.1144/1467-7873/08-184

Xu, J., Ciobanu, C. L., Cook, N. J., et al., 2016. Skarn Formation and Trace Elements in Garnet and Associated Minerals from Zhibula Copper Deposit, Gangdese Belt, Southern Tibet. *Lithos*, 262: 213–231. https://doi.org/10.1016/j.lithos.2016.07.010

Yin, A., Harrison, T. M., 2000. Geologic Evolution of the Himalayan-Tibetan Orogen. *Annual Review of Earth and Planetary Sciences*, 28(1): 211–280. https://doi.org/10.1146/annurev.earth.28.1.211

Yousefi, M., 2017. Recognition of an Enhanced Multi-Element Geochemical Signature of Porphyry Copper Deposits for Vectoring into Mineralized Zones and Delimiting Exploration Targets in Jiroft Area, SE Iran. *Ore Geology Reviews*, 83: 200–214. https://doi.org/10.1016/j.oregeorev.2016.12.024

Yousefi, M., Carranza, E. J. M., 2015. Fuzzification of Continuous-Value Spatial Evidence for Mineral Prospectivity Mapping. *Computers & Geosciences*, 74: 97–109. https://doi.org/10.1016/j.cageo.2014.10.014

Yousefi, M., Carranza, E. J. M., Kamkar-Rouhani, A., 2014. Weighted Drainage Catchment Basin Mapping of Geochemical Anomalies Using Stream Sediment Data for Mineral Potential Modeling. *Journal of Geochemical Exploration*, 128: 88–96. https://doi.org/10.1016/j.gexplo.2013.01.013

Yousefi, M., Kamkar-Rouhani, A., Carranza, E. J. M., 2012. Geochemical Mineralization Probability Index (GMPI): A New Approach to Generate Enhanced Stream Sediment Geochemical Evidential Map for Increasing Probability of Success in Mineral Potential Mapping. *Journal of Geochemical Exploration*, 115: 24–35. https://doi.org/10.1016/j.gexplo.2012.02.002

Yousefi, M., Kamkar-Rouhani, A., Carranza, E. J. M., 2013. Application of Staged Factor Analysis and Logistic Function to Create a Fuzzy Stream Sediment Geochemical Evidence Layer for Mineral Prospectivity Mapping. *Geochemistry*: *Exploration*, *Environment*, *Analysis*, 14(1): 45–58. https://doi.org/10.1144/geochem2012-144

Yousefi, M., Kreuzer, O. P., Nykänen, V., et al., 2019. Exploration Information Systems—A Proposal for the Future Use of GIS in Mineral Exploration Targeting. *Ore Geology Reviews*, 111: 103005. https://doi.org/10.1016/j.oregeorev.2019.103005

Zhang, S. R., 2007. The Research of Method of Geochemical Element Spatial Quantitative Association and Visualization: [Dissertation]. Jilin University, Changchun. 1–118 (in Chinese with English Abstract)

Zhang, S. Z., Gao, S. B., Zhang, Y. C., et al., 2017. Geochronology and Geochemistry of the Ore-Bearing Intrusion in the Longgen Lead-Zinc Deposit in Tibet and Its Geological Significance. *Acta Geologica Sinica*: *English Edition*, 91(s1): 105–106. https://doi.org/10.1111/1755-6724.13208

Zhang, Y. C., Gao, S. B., Zheng, Y. Y., et al., 2018. Mineralogy, Fluid Inclusions and C-H-O-S-Pb Isotopes of the Palaeocene Longgen Pb-Zn Deposit in the Western Nyainqentanglha Belt, Tibet. *Ore Geology Reviews*, 102: 18–43. https://doi.org/10.1016/j.oregeorev.2018.08.026

Zhao, H., Yang, J. S., Liu, F., et al., 2019. Post-Collisional, Potassic Volcanism in the Saga Area, Western Tibet: Implications for the Nature of the Mantle Source and Geodynamic Setting. *Journal of Earth Science*, 30(3): 571–584. https://doi.org/10.1007/s12583-019-1228-7

Zhao, J. N., Chen, S. Y., Zuo, R. G., 2016. Identifying Geochemical Anomalies Associated with Au-Cu Mineralization Using Multifractal and Artificial Neural Network Models in the Ningqiang District, Shaanxi, China. *Journal of Geochemical Exploration*, 164: 54–64. https://doi.org/10.1016/j.gexplo.2015.06.018

Zhu, D. C., Zhao, Z. D., Niu, Y. L., et al., 2011. The Lhasa Terrane: Record of a Microcontinent and Its Histories of Drift and Growth. *Earth and Planetary Science Letters*, 301(1/2): 241–255. https://doi.org/10.1016/j.epsl.2010.11.005

Zuo, R. G., 2011. Identifying Geochemical Anomalies Associated with Cu and Pb-Zn Skarn Mineralization Using Principal Component Analysis and Spectrum-Area Fractal Modeling in the Gangdese Belt, Tibet (China). *Journal of Geochemical Exploration*, 111(1/2): 13–22. https://doi.org/10.1016/j.gexplo.2011.06.012

Zuo, R. G., 2014. Identification of Geochemical Anomalies Associated with Mineralization in the Fanshan District, Fujian, China. *Journal of Geochemical Exploration*, 139: 170–176. https://doi.org/10.1016/j.gexplo.2013.08.013

Zuo, R. G., Carranza, E. J. M., Wang, J., 2016. Spatial Analysis and Visualization of Exploration Geochemical Data. *Earth-Science Reviews*, 158: 9–18. https://doi.org/10.1016/j.earscirev.2016.04.006

Zuo, R. G., Cheng, Q. M., Agterberg, F. P., et al., 2009. Application of Singularity Mapping Technique to Identify Local Anomalies Using Stream Sediment Geochemical Data, a Case Study from Gangdese, Tibet, Western China. *Journal of Geochemical Exploration*, 101(3): 225–235. https://doi.org/10.1016/j.gexplo.2008.08.003

Zuo, R. G., Wang, J., 2016. Fractal/Multifractal Modeling of Geochemical Data: A Review. *Journal of Geochemical Exploration*, 164: 33–41. https://doi.org/10.1016/j.gexplo.2015.04.010